12-2016

Color, Color Pattern, Habitat Use, and Morphology of *Anolis conspersus*

Christopher Ryan Peterson
University of Tennessee, Knoxville, cpeter22@vols.utk.edu

To the Graduate Council:

I am submitting herewith a thesis written by Christopher Ryan Peterson entitled "Color, Color Pattern, Habitat Use, and Morphology of *Anolis conspersus*." I have examined the final electronic copy of this thesis for form and content and recommend that it be accepted in partial fulfillment of the requirements for the degree of Master of Science, with a major in Ecology and Evolutionary Biology.

Arthur C. Echternacht, Major Professor

We have read this thesis and recommend its acceptance:

Benjamin M. Fitzpatrick, Daniel Simberloff

Accepted for the Council:
Carolyn R. Hodges

Vice Provost and Dean of the Graduate School

(Original signatures are on file with official student records.)

Color, Color Pattern, Habitat Use, and Morphology of *Anolis conspersus*

A Thesis Presented for the

Master of Science

Degree

The University of Tennessee, Knoxville

Christopher Ryan Peterson

December 2016

Acknowledgements

I would like to thank everyone who as assisted or advised me throughout the long process of preparing this thesis. My advisors and committee members (Sandy Echternacht, Ben Fitzpatrick, and Dan Simberloff) have guided me in the specifics of my research and helped me develop my ability to to think about ecological and evolutionary questions as a whole.

The Cayman Islands Department of the Environment (DoE) authorized my research permit; members of the DoE staff provided conslutation and logstical support, particularly Research Officers Jessica Harvey and Jane Haakonsson. Paul Watler, Environmental Programmes Manager of the National Trust for the Cayman Islands, made it possible for me to work on lands administered by the Trust. Laura Casolino, Doug Bell, and Krista Mougey provided essential assistance with field collection and helped me locate suitable sampling sites. Fred Burton has long supported research on endemic species of the Cayman Islands and provided connections the previously mentioned individuals and institutions who were necessary to complete this work.

My colleagues and friends in the Ecology and Evolutionary Biology department have helped me come up with new ideas, improve my skill set, and maintain my sanity over the past three years. In particular, Jim Fordyce, Zach Marion, Todd Pierson, Cassie Dresser, and Evin Carter have helped me variety of post-fieldwork difficulties. Funding for this research was provided by the University of Tennessee EEB Department. Finally, I would like to thank my parents, Mark Peterson and Nancy Brown-Peterson, for providing feedback on my research and continued support throughout my graduate education and beyond.

Abstract

Understanding color polymorphism and associated ecological and morphological divergence is important to improving out knowledge of diversity and speciation; anoles are a model clade for addressing these questions. *Anolis conspersus* (the Grand Cayman blue-throated anole) is endemic to a small island and has color variants (green, blue, and brown morphs) that are spatially arranged despite a lack of wider environmental gradients. I examined aspects of ecological and morphological variation among and within *A. conspersus* populations throughout Grand Cayman to evaluate potential divergence between color morphs. No substantial differences in habitat use or morphology were detected. The blue and green morphs were difficult to categorize, suggesting the *A. conspersus* color system is more complicated than previously believed.

Table of Contents

List of Tables

List of Figures

1 Introduction

1.1 Color polymorphism

Developing a deeper knowledge of the ecological and evolutionary context of color polymorphism is an important component to understanding the diversity of life. Color variants are often associated with other intraspecific differences in morphology, ecology, and behavior. For example, Midas cichlids (*Amphilophus citrinellus* species complex) have gold and dark morphs, with golden individuals having larger body size, stronger pharyngeal jaws, and different diet than their dark conspecifics (Kusche et al., 2015). Variation in throat pigmentation among side-blotched lizards (*Uta stansburiana*) is connected to substantial differences in social behavior (Sinervo et al., 2001), and white-throated sparrows (*Zonotrichia albicollis*) exhibit differences in reproductive strategy between individuals with white-striped or tan-striped head plumage (Tuttle, 2003). In situations where a species occupies a variety of habitat types, different colors can provide more effective crypsis in some areas than others, leading to maintenance of the polymorphism by selection. This has been observed in a wide variety of animals, including Northern cricket frogs (*Acris crepitans;* Caldwell, 1982), grove snails (*Cepaea nemoralis;* Cook, 2008), and mottled rock rattlesnakes (*Crotalus lepidus*; Farallo and Forstner, 2012). Ultimately, traits associated with color polymorphism may lead to reduced gene flow and eventual speciation (Gray and McKinnon, 2007).

Color polymorphism can exist even across very small islands. For example, Asian spiny-back spiders (*Thelacantha brevispina*) on Mo'orea (134 km^2) exhibit a variety of color variants, with lighter morphs generally occurring near coastal, low-canopy areas and darker morphs occurring in the forest (Truong, 2012). The endemic Inaccessible Island (14 km^2) bunting (*Neospiza acunhae*) has distinct lowland and upland morphs,

where high elevation birds have more intense yellow coloration (Ryan et al., 1994). The Skyros (223 km^2) wall lizard (*Podarcis gaigeae*) has orange, yellow, and white throat color morphs (along with intermediates) that frequently co-occur in the same in the same population; these are believed to be involved in social signaling (Runemark et al., 2010). Most examples of color polymorphisms are believed to be maintained across such a small spatial scale because they are adaptive to different environmental factors or are under sexual selection.

Anole lizards (Dactyloidae: *Anolis*) are a model system for studying variation in habitat use, morphology, and coloration both within and among species (Losos, 1994). The genus contains about 360 species distributed across the West Indies, South America, and Central America (Losos, 2011). Sympatric populations often partition structural habitat by perch height or perch diameter. This partitioning is associated with changes in body size and limb length, with larger lizards preferring larger branches. These associations are particularly pronounced in the Greater Antillies. Communities of anole species on each of these large islands have independently evolved similar sets ecomorphs, each of which is specialized for using a specific structural habitat (Williams, 1972; Losos et al., 1998).

Smaller islands are limited to one or two species, with substantial divergence in body size on the two-species islands. On several single-anole islands, substantial intra-specific variation in morphology or habitat use is present. For example, *A. oculatus* (native to Dominica) exhibits large amounts of ecological divergence, with associations between body coloration, morphological characters, geographic patterns, and environmental conditions (Malhotra and Thorpe, 1997). The Guadeloupean leopard anole (*A. marmoratus*) displays striking variation in coloration that is associated with elevation and precipitation gradients (Muñoz et al., 2013). A similar trend exists on Martinique

with *A. roquet* (Thorpe and Stenson, 2003). Each of these species inhabits geographically complex islands with substantial variation in elevation and climate.

1.2 *Anolis conspersus*

Anolis conspersus (the Grand Cayman blue-throated anole; Garman, 1887) exhibits substantial variation among populations with respect to color and patterning of adult males despite living on a small, relatively flat island. This anole is endemic to Grand Cayman and is the only anole native to the island. However, an invasive population of *A. sagrei*, thought to have originated from Florida (Kolbe et al., 2007), has been present on the island since at least the early 1980's (Minton and Minton, 1984). The invasive species now occurs over much of the island.

Jackman et al. (2002) hypothesized the species arose from colonization of Grand Cayman by *A. grahami*, a Jamaican trunk-crown anole, two to three million years ago. Its range encompasses the entirety of the island, with two recognized subspecies: *A. c. conspersus* and *A. conspersus lewisi* (Grant and Lewis, 1940). The species exhibits extreme sexual size dimorphism, with males exhibiting larger snout-vent length and head length than females. Similar, though less extreme, dimorphism has been observed in other anoles on islands lacking congeneric competitors and is thought to allow for inter-sexual resource partitioning (Schoener, 1967).

Despite the small size of Grand Cayman, *A. conspersus* exhibits substantial variation in male body coloration. Three distinct color morphs are distributed along the precipitation gradient (Macedonia, 2001). The green morph (corresponding to *A. c. conspersus)* is found in the southwestern corner of the island, where precipitation and development are greatest. While it historically ranged across much of western Grand

Cayman (Grant and Lewis, 1940), more recent accounts have limited it to small enclaves in the capital of Georgetown that are completely surrounded by blue morph populations (Macedonia and Clark, 2001). This morph is lightly spotted, with bright green to yellowish-green coloration on the dorsum, legs, and tail, the green often transitioning towards blue near the venter. The green morph is the most visually similar to *A. grahami.*

The brown morph (*A. c. lewisi*) inhabits the eastern quarter of the island, where precipitation is lowest. It is primarily brown, with a teal tail, hints of blue on the legs, and a vermiculated pattern.

The blue morph (which corresponds to no described subspecies) occupies most of the rest of the island, including large areas previously occupied by *A. c conspersus*; its range limits are somewhat fuzzy, and it sometimes co-occurs with individuals from the other two morphs. Its coloration is highly variable, although it is spotted and consistently possess a blue tail, sides, and legs. Some individuals have a light brown dorsal coloration, with heads that range from blue to yellow. Despite the breadth of its current distribution, the blue morph was not described in scientific literature until 1980's (Macedonia, 2001).

Macedonia and Clark (2001) have suggested the blue morph may be the result of a reduced-melanin variant of the brown morph that expanded West and hybridized with green populations. All morphs are capable of rapidly changing to a dark shade of brown (metachrosis) and have a bright blue dewlap that extends into the ultraviolet spectrum. Given that dewlap color is a consistently associated with species recognition across *Anolis* (Losos, 2011), communication among morphs is likely not restricted, although there is some variation in headbob displays (Macedonia and Clark, 2001).

The evolutionary cause of the *Anolis conspersus* color morphs is currently un-

known. A spectral analysis of the three morphs showed that the primary coloration is at least somewhat cryptic in ambient lighting conditions, which suggests a possible adaptive explanation of this variation (Macedonia, 2001). Male color morphs may also be a result of differing patterns of sexual selection across the island; however, most evidence for sexual selection in anoles focuses on dewlap color (Sigmund, 1983) or morphology (Butler and Losos, 2002). The different morphs may have also arisen from neutral genetic processes. Regardless of their evolutionary origin, other variation among the color morphs has been mostly unstudied.

1.3 Objectives

The goal of the study reported here was to investigate whether the color morphs of *Anolis conspersus* exhibit differences in habitat use or morphology. If this is the case, I would expect morphological or habitat use traits to predict color pattern better than a model that considers only spatial location. Consistent differences in habitat use or morphology might suggest that *A. conspersus* is beginning to exhibit a similar pattern to anoles on multi-species islands.

2 Methods

2.1 Study sites

Grand Cayman is a 196 km^2 island which is located 435 km south of Cuba and 438 km west of Jamaica. The Cayman Bluff formation group, which includes most of the eastern portions of Grand Cayman and the Southern ridge, arose 30 mya and consists mainly of dolostone; the remainder of the island formed in the Pleistocene (Jones, 1994). Although the size of the island would have changed with sea level shifts, there is no evidence that Grand Cayman was ever fragmented into more than one island. Many areas are covered in jagged phytokarst. The island has little variation in elevation, with the highest point being only eighteen meters above sea level. Precipitation varies geographically across the island, with high rainfall in the southwest corner that decreases to the north and the east (Burton, 1994). The island has become increasingly developed during the late twentieth century, with human activity disproportionately affecting the western side of the island. Vehicular traffic could facilitate anole relocation around the island.

To adequately survey the population of *A. conspersus,* I sampled 19 sites across Grand Cayman between June and August 2014 (Table A.1; Figure B.1). Distances among sites were substantially greater than typical anole dispersal ranges (Losos, 2011), although long-distance vehicular-assisted migration among sites near roadways could reduce the effective distance among sites and increase gene flow.

2.2 Data collection

I captured 16 adult males at each of the 19 sample sites (Figure 1). At the spot each lizard was initially sighted, I measured habitat use characteristics. Perch height (PH; cm) and perch diameter (PD; cm) were measured with a Lufkin Engineers 2m metric/English folding ruler; perch temperature (PT; °C) was recorded with a Miller & Weber, Inc. Cloacal Thermometer 1 cm above the perch; ambient air temperature (AT; °C) and relative humidity (RH) were recorded 1 m from perch with a shaded Forestry Suppliers Non-Mercury Pocket Sling Psychrometer; perch texture and shade level were qualitatively described. Lizards were returned to a controlled environment, where I measured mass (M; g) with a Pesola Micro-Line 20030 30g capacity Precision Scale) and snout-vent length (SVL; mm), tail length (TL; mm), and hind limb length (HLL; mm) with a ruler. Hind limb length was measured as the distance from distal tip of the claw on metatarsal IV to the insertion of the limb into the body wall (Kolbe and Losos, 2005). Each lizard was photographed under consistent temperature and lighting conditions with a Nikon D5200 DSLR camera. The GPS coordinates were recorded for each capture location with a Garmin eTrex H GPS, and lizards were returned to their original locations within 24 hours.

2.3 Data processing

Each continuous predictor variable (SVL, TL, HLL, M, PH, PD, AT, and RH) was normalized to a mean of zero and standard deviation of one. This reduces the correlation between slopes and the intercept and allows for model coefficients to be easily comparable, since they now represent the effect of an increase in the predictor by one standard deviation. Prior to normalization, HLL and TL were corrected for body

size and TL was corrected for tail loss; this was done by regressing the HLL against SVL and regressing TL against SVL and an indicator of whether the tail had been autotomized. The residuals of these regression were retained as the corrected values of TL and HLL.

Other measurements were categorized as follows: shade (S; None/Partial/Full), perch texture (TEX; smooth/semi-smooth/rough), perch material (PM; whether the lizard was perched on a branch, a trunk or an artificial object), perch angle (PA; whether the lizard's head was facing down/sideways/up), and perch connectivity (PC; sparsely or heavily connected). Two-level variables were coded as 0 or 1 and three-level variables were coded as 2 dummy variables, where the three levels were represented by (0,0), (1,0), and (0,1). This resulted in a total of 18 predictor variables.

I attempted a variety of methods to quantitatively assess anole dorsal coloration from the photographs; none of these produced consistent, interpretable results. Eventually, I categorized the lizards as spotted or vermiculated as a proxy for color. The dorsal pattern was essentially binary (no individuals were intermediates) and could be easily classified by visual inspection.

In order to control for the effect of geography, I calculated pairwise distances between sites. Because anoles are far more likely to disperse across land than over water, these distances need to be constrained to the island's landmass. This was accomplished with resistance mapping (using the gdistance package in R; van Etten, 2015): I divided Grand Cayman into a grid of one square-meter cells, assigned land cells a resistance of 1, and designated water as uncrossable. The least-cost path among sites was then calculated, and the resulting paths were rescaled so that the smallest distance between sites was one. To account for site-level precipitation, I extracted and normalized the average annual rainfall at each site from the WorldClim Bioclim12 interpolated climate

dataset (Hijmans et al., 2005). All data were processed in R version 3.1.2 (R Core Team, 2016).

To assess the ability of habitat use or morphology to predict dorsal pattern, I used hierarchical Bayesian models with pattern (spotted or vermiculated) as the response variable and habitat use and morphological variables as the predictors. This model is essentially a logistic regression that has been modified to account for variation among sites and control for multiple comparisons. Two variations of this model were run, one of which accounts for spatial autocorrelation among sites and one which does not. In the next section, I describe how and why the logistic regression was adjusted to more accurately model the data collection process. Tables A.2 and A.3 contains a list of symbols used in these models, and the full model description is available in Appendix C. I used a second model to robustly estimate how the means of each continuous predictor varied among sites and whether they were associated site precipitation; symbols used in this model are listed in Table A.4.

2.4 Model descriptions and justifications

Logistic regression (Figure B.2) assumes that a binary response variable $\boldsymbol{Y}$ is predicted by a Bernoulli distribution with parameter $\boldsymbol{p}$, a value between 0 and 1. This parameter is logit transformed into $\boldsymbol{\eta}$ ($\text{logit}(p_i) = \log\frac{p_i}{1-p_i} = \eta_i$), which can take any real value and represents the natural logarithm of the odds of $Y_i = 1$. Predictor variables ($\boldsymbol{X}$) are incorporated as $\eta_i = \beta_0 + \boldsymbol{\beta}\boldsymbol{X}_i$, where β_0 is the intercept (the baseline log-odds) and $\boldsymbol{\beta}$ is a vector of slope coefficients that represent the effects of the predictors. Because $\boldsymbol{\eta}$ is on a logistic scale, additive components of η_i have a nonlinear effect on p_i; thus, the influence of a given β coefficient on p depends on the values of the intercept

and the other slopes.

2.4.1 Accounting for site-level variation

The base model assumes that there is no variation in the intercept or slopes among sites, which is unrealistic for this sampling approach. I could address this by modeling each site separately; however, this would assume that each population is entirely independent and shared no underlying association. This approach would also severely reduce sample sizes, magnifying uncertainty and increasing the chance for spurious results. A better approach is to use a hierarchical model that partially pools information across sites (Figure B.3). The simplest way to do this is to model $\beta_{j,k}$ (the coefficient for predictor k in site j) as normally distributed around a grand coefficient μ_k with standard deviation σ_k. This standard deviation represents the degree to which the effect of predictor k varies among sites; $\beta_{j,k}$ converges to μ_k (a single-slope model) as σ_k approaches 0, and each $\beta_{j,k}$ becomes independent of the others as σ_k approaches ∞. Each σ_k was modeled with a folded Cauchy distribution that shared a common scale parameter τ_σ (Gelman, 2006). The folded (or half) Cauchy distribution (equivalent to a folded Student-t distribution with 1 degree of freedom) is similar to a normal distribution limited to non-negative values but with more probability density in the tail; essentially, it prefers small values but allows for large ones. Because the half Cauchy's scale parameter is also its median, the hyperparameter τ_σ models the median variation in β-coefficients among sites. τ_σ was given a half Cauchy prior distribution with a scale of 1, so that it could vary among a variety of reasonable options but would prefer smaller values.

Modeling $\beta_{j,k}$ with a normal distribution assumes that there is no relationship between the value of the different β coefficients at each site (McElreath, 2016). Each

site's coefficients ($\boldsymbol{\beta}_j$) were modeled with a multivariate normal distribution with mean vector $\boldsymbol{\mu}$ and a covariance matrix $\boldsymbol{\Sigma}$, which can be decomposed into the variance of each coefficient ($\boldsymbol{\sigma}^2$) and a correlation matrix $\boldsymbol{\Omega}$. The correlation matrix is given a prior distribution developed by Lewandowski, Kurowicka, and Joe (LKJ; 2009) that has a single parameter, ϕ. This LKJ prior can be best understood as a combination of beta distributions (one for each pairwise combination of predictors) that are rescaled from $(0, 1)$ to $(1, 1)$, where both parameters are equal to ϕ. Thus, the probability of an identity matrix (i.e., no correlation) increases as ϕ grows larger than 1, the probability of a highly correlated matrix increases as ϕ approaches 0, and the probability is uniform across all valid correlation matrices when $\phi = 1$. I fixed the LKJ parameter at $\phi = 2$, which provides light regularization towards uncorrelated coefficients without preventing tight covariance.

2.4.2 Controlling for multiple comparisons

Spurious associations (i.e., false positives) are a serious concern when modeling the effects of 18 predictors across 19 sample sites with limited data. Regularization methods, such as lasso (Tibshirani, 1996) and elastic net (Zou and Hastie, 2005), are common regression techniques when it is assumed that most of the predictors have small effects, but a few may be large (Figure B.4). These techniques will shrink coefficients to zero or near-zero unless the coefficient's predictor provides a strong signal in the data. Thus, they act as a form of automatic Bayesian model selection and averaging. Hierarchical shrinkage priors (which include HS_ν, HS_ν^+, and horseshoe priors) are a particularly efficient class of regularization methods that use both a global scale parameter (τ_λ), which ensures that most coefficients are shrunk to near zero, and local scale parameters (λ_k), which allows specific coefficients to counteract this shrinkage

(Carvalho et al., 2010). The grand coefficients (μ_k) were modeled with HS_3^+ priors (Bhadra et al., 2015): μ_k was drawn from a normal distribution with a mean of 0 and a standard deviation of λ_k; each λ_k is the product of two parameters ($\lambda_{k,1}$ and $\lambda_{k,2}$) which have independent half student-t distribution with 3 degrees of freedom and a shared standard deviation of $\sqrt{\tau_\lambda}$. τ_λ has a half Cauchy distribution scaled by the reciprocal of the number of predictors.

2.4.3 Incorporating the precipitation gradient

Because the distribution of *Anolis conspersus* color morphs is associated with Grand Cayman's precipitation gradient (Figure 1), the site-level intercepts ($\beta_{j,0}$) are almost certainly affected by rainfall. This can be incorporated into the model by designating a new intercept vector ($\beta^*_{j,0}$), where $\beta^*_{j,0} = \beta_{j,0} + \gamma Z_j$, where Z_j is the normalized average annual precipitation for site j, and γ is the regression coefficient for Z. γ was modeled as normally distributed around 0 with a standard deviation of ξ; ξ was modeled as a half-Cauchy with a scale of 2.5. With this modification, $\beta_{0,j}$ now represents the baseline site-level variation that is not associated with rainfall (Figure B.5).

2.4.4 Accounting for spatial autocorrelation

The previously described model assumes that variation among sites is not affected by geographic distance. While much of the geographic distribution is likely associated with precipitation, this would not capture other spatial patterns. A spatially structured model assumes that sites are more similar to nearby sites than to distant ones (Plant, 2012); this could be relevant, given that interactions among sites would be limited by dispersal. I expanded the non-spatial model by assuming the matrix of β coefficients are distributed by a matrix-normal distribution; this distribution gener-

alizes the multivariate normal by adding a second covariance matrix ($\mathbf{\Psi}$) that accounts for among-site variation, where $\Psi_{j,j'} = \exp(\frac{-D^2_{j,j'}}{\ell^2})$ (Figure B.6). This covariance matrix follows a Gaussian (or squared exponential) kernel, which is a smooth function of the pairwise distance between the sites ($D_{j,j'}$) and a length scale parameter (ℓ) that accounts for the maximum distance that spatial autocorrelation is relevant. As ℓ approaches zero, Ψ becomes an identity matrix (that is, uncorrelated). I modeled ℓ with a half Cauchy prior (scale = 1). This assumes that spatial correlation probably decays rapidly but still maintains a relatively high probability of long-distance autocorrelation.

2.4.5 Hierarchical trait means model

I developed a separate hierarchical model to examine trait variation among sites. In this model, a continuous trait (X_i) was modeled with a t_7 distribution around site mean $\alpha_{j|i}$ with a dispersion of $\varepsilon_{j|i}$. The t distribution has heavier tails than a normal distribution, making the estimate more robust to outliers; these heavy tails also mean that ε_j is not a true standard deviation parameter, although it serves the same function. The ε parameters were modeled as half-Cauchy distributions with a common scale term (τ_ε); this allows sites to have different variances while still partially pooling some information. The site level mean α_j is normally distributed around an expected value of θ_j with a standard deviation of τ_α. θ_j is the sum of the grand mean (ω), and the effect of precipitation (δZ_i). I assigned δ a normal prior with a mean of 0 and a standard deviation of τ_δ. It is typical to give top-level hyperparameters such as ω a prior distribution centered on 0; however, even a cursory glance at the data reveals this to be a very poor choice. Instead, I used a weakly informative normal distribution for ω, with a mean of $c_x = \text{median}(X)$ and standard deviation of $q_x = \text{range}(X) * 0.25$; this provides an appropriate location and scale for the data. Likewise, the scale hyperparameters (τ_α,

τ_ϵ, and τ_δ) received half-Cauchy priors with a scale of q_x.

This model was run on the non-normalized values of each of the continuous traits measured (SVL, TL, HLL, M, PH, PD, AT, and RH). Only individuals with complete tails were included in the TL model.

2.4.6 Model implementation

All models were implemented in Stan (Gelman et al., 2015), a probabilistic programing language for Bayesian inference with Hamiltonian Monte Carlo (HMC), a Markov chain Monte Carlo (MCMC) variant that uses simulated Hamiltonian dynamics to estimate the posterior distribution of the parameters (Betancourt and Girolami, 2015). The models were coded with non-centered parameterizations (Papaspiliopoulos et al., 2007) for increased efficiency. Each model was run with 6 independent chains for 2500 steps each, with the first 1500 iterations used for adaptive warmup and the last 1000 iterations retained. Because HMC is substantially more efficient at producing uncorrelated samples than other MCMC methods, fewer iterations were necessary for an adequate effective sample size (Hoffman and Gelman, 2011). Convergence was checked with the Rubin-Gelman diagnostic statistic ($\hat{R}$; Gelman et al., 2013) and by graphically checking trace plots. The models were also assessed with posterior predictive checks. Prior sensitivity was assessed by re-running the models when varying the magnitude of the τ, ϕ, and q_x hyperparameters and by replacing the Gaussian spatial covariance function with an exponential kernel ($\Psi_{j,j'} = \exp(\frac{-D_{j,j'}}{\ell})$); the parameter estimates of these re-runs were compared against the original output for consistency.

3 Results

The intercepts (Figure B.7) varied substantially among sites in both the spatial (SP) and non-spatial (NSP) pattern models, which both exhibited an east-west pattern that matches the known distribution of colors. There was a strong negative effect of precipitation (γ) on site-level intercepts, with lower precipitation predicting vermiculated individuals. This was more pronounced in the NSP model.

The pattern models slopes all contained 0 within the posterior distribution's 50% high density interval (HDI; Figures B.8-9). Additionally, the intercepts had substantially larger magnitudes than the slopes at most sites. Because of the non-linearity of the logit-scale parameters, this means that none of the normalized predictors have a meaningful effect on p_i over their range of possible values. Therefore, none of the measured traits were useful in predicting pattern. There was little variation in slope estimates among sites. This is likely because many of the sites tended to consist entirely of one pattern, which would not provide enough information estimate different slopes, resulting in the site-level coefficient shrinking to the overall slope.

Site-level trait means had little to no association with precipitation (Figure B.10). AT had a slight negative association with precipitation, and RH had a positive association; however, the 95% high-density intervals (HDI) of their δ both contained 0, so the association is uncertain. Both the 95% and 50% HDIs of the δ coefficients for the other 6 traits included 0, indicating a low probability of association with precipitation. Site-level means varied among sites for SVL (Figure B.11), TL (Figure B.12), M (Figure B.13), HLL (Figure B.14), AT (Figure B.15), and RH (Figure B.16). PH (Figure B.17) and PD (Figure B.18).

4 Discussion

The association between pattern and precipitation follows the well-documented spatial distribution of color morphs across the island. I detected no connection between the dorsal patterning of adult male *Anolis conspersus* and their habitat use or morphology. In particular, perch height and diameter exhibited an essentially uniform distribution that did not vary with location, precipitation, or pattern (Figures B.17-18). It therefore appears that adult male *A. conspersus* use whatever structural habitat is available. The potential associations of relative humidity and ambient air temperature (Figures B.15-16) with precipitation levels are also plausible, given that both variables are affected by rainfall. Although some spatial variation was apparent for the morphological traits traits (Figures B.11-14), these did not exhibit any consistent spatial patterns, and could represent either natural inter-population variation or the effect of an unmeasured covariate such as food abundance or human impacts. It is possible that greater variation may exist within female anoles, which tend to have smaller body sizes and lower perches than males. Females and juveniles were excluded from this study because females do not exhibit the same pattern of color morph variation, and males only begin to express their coloration as older juveniles; both groups are harder to detect and collect than adult males, which would have resulted in an unusable sample size. There are also other traits that I did not measure which could exhibit substantial variation. Alternatively, Grand Cayman may be too small and flat to support this variation.

Precipitation levels, vegetation type, and body coloration all vary spatially across the island. It is therefore challenging to control for spatial autocorrelation in an analysis without possibly erasing the effects of interest. The confounding of space and precipitation is a plausible explanation for why the SP model's γ 95% HDI included 0 while

the NSP model's did not; some of the variation accounted for by precipitation in the NSP model was explained by spatial autocorrelation in the SP model. Preexisting GIS climate layers (such as WorldClim) are suboptimal for problems of this scale because a) they are created from datasets that only contain one or two points within the area of interest (Hijmans et al., 2005), and b) the climate data may substantially pre-date the time period during which the study's data were collected. The precipitation data I used was therefore heavily influenced by the assumptions of interpolation model. While I am confident enough in the sign of the estimated γ coefficients, I am hesitant to trust the magnitude. More granular precipitation data collected from numerous rain gauges across the island would be necessary to properly estimate γ and δ. Such data were collected (summarized by Burton, 1994), but the records have apparently been destroyed (F.J. Burton, pers. com.).

Grand Cayman has undergone substantial human alteration over the past decades, including species introductions (such as *Anolis sagrei, Iguana iguana,* and numerous domestic and agricultural animals; for reptiles, see Echternacht et al., 2011) and habitat alteration associated with development. In particular, distant portions of the island are now much more connected, with large numbers of construction and waste management vehicles traveling all across the island. Anoles could easily be transported to distant portions of the island, allowing for population intermixing and the reduction of any local variation. This could be a possible explanation the results at site K, where the odds of an individual being spotted or vermiculated were even. This particular area was associated with a conservation group that had frequent vehicle transportation to and from the Eastern side of the island, which could allow hitchhiking anoles to disrupt the expected patterns.

It is possible that habitat use variation may have been present among color

morphs, but has disappeared since the invasion of Grand Cayman by *Anolis sagrei.* There is some evidence that *A. conspersus* of both sexes shift to higher perches in the presence of *A. sagrei* (Losos et al., 1993), which could have subsequent effects on other morphological and habitat use traits. Because *A. sagrei* were not of primary research concern, I do not have any reliable estimate of their abundance at each site; however, I did not observe substantial numbers of *A. sagrei* in any but the most disturbed areas (e.g., near sites D, F, and L).

Many of the individuals sampled did not fit nicely into the three *A. conspersus* color morphs that have been discussed in the literature. Since simple categorization by color was not possible, I initially attempted to quantify the lizard color from white-balanced photographs. Because the lizards were alive during photography and too much restraint would have induced stress-related color shifts, there was no way to maintain consistency in anole angles and positions between the photographs. As a result, the data directly extracted from the images contained too much noise to be useful. I ultimately chose dorsal patterning as the response because it could consistently distinguish the brown morph from the blues and greens.

Individuals of the "brown" morph were most easily distinguished by the presence of vermiculations instead of spots; actual dorsal coloration was generally a light gray or tan, sometimes with powder blue on the sides and tail. "Blue" and "green" individuals were much harder to distinguish, with a number of lizards having patches of both colors. Head coloration in the western anoles was also highly variable, with some individuals having large yellow patches that extended down to the neck and were occasionally flecked with blue or green. I have also received credible reports of individual anoles changing between blue and green over time (F.J. Burton, pers. com.). Grant and Lewis (1940) described the dorsal coloration of *A. c. lewisi* as "brownish to olive-colored;" I

saw no evidence of olive coloration in any lizards.

The relationship of the blue morph to the described subspecies (the green *A. c. conspersus* and the brown *A. c. lewisi*) remains uncertain. Macedonia (2001) suggested that the blue morph is derived from the brown morph, which lost is vermiculations and acquired new coloration as it expanded westward. The difficulty of distinguishing between the blue and green morphs suggests that the the two may in fact be a single color morph with a wide degree of individual variation. Alternatively, these ambiguities could be an indication of interbreeding between previously distinct color morphs. *Anolis c. conspersus* and *A. c. lewisi* may even have originated from introductions from separate *A. grahami* subpopulations. The descriptions of the morphs themselves have changed over time (e.g., Garman 1887; Grant and Lewis 1940; Schoener 1967; Losos et al. 1993; Macedonia 2001); this is particularly notable for the blue morph, which did not appear at all in early descriptions and yet became the most widely distributed color some time between the 1940's and 1980's. A consistent, long-term survey of color morph variation and distribution could be very helpful in understanding if and how the morphs are changing.

Examining the population genetics of *Anolis conspersus* will be an important next step in understanding the variation within this species. I took tissue samples from each individual sampled and will be working with collaborators to examine the genetic structure of *A. conspersus*, allowing for comparisons among populations that could determine wether or not genetic patterns are concordant with the geographical patterns of morphology, color, color patterns, or habitat. The results of this future work will hopefully provide a concrete explanation for how Grand Cayman is able to support this variation within *Anolis conspersus.*

Literature Cited

Betancourt, M. and Girolami, M. 2015. Hamiltonian Monte Carlo for hierarchical models. CRC Press, Boca Raton, FL.

Bhadra, A., Datta, J., Polson, N. G., and Willard, B. 2015. The Horseshoe+ Estimator of Ultra-Sparse Signals. *arXiv:1502.00560 [math, stat]* . arXiv: 1502.00560.

Burton, F. J. 1994. Climate and tides of the Cayman Islands, pp. 51–60. *In* M. A. Brunt and J. E. Davies (eds.), The Cayman Islands, number 71 in Monographiae Biologicae. Springer Netherlands. DOI: 10.1007/978-94-011-0904-8_3.

Butler, M. A. and Losos, J. B. 2002. Multivariate Sexual Dimorphism, Sexual Selection, and Adaptation in Greater Antillean *Anolis* Lizards. *Ecological Monographs* 72:541–559.

Caldwell, J. P. 1982. Disruptive selection: a tail color polymorphism in *Acris* tadpoles in response to differential predation. *Canadian Journal of Zoology* 60:2818–2827.

Carvalho, C. M., Polson, N. G., and Scott, J. G. 2010. The horseshoe estimator for sparse signals. *Biometrika* p. asq017.

Cook, L. M. 2008. Variation with habitat in *Cepaea nemoralis*: the Cain & Sheppard diagram. *Journal of Molluscan Studies* 74:239–243.

Echternacht, A. C., Burton, F. J., and Blumenthal, J. M. 2011. The amphibians and reptiles of the Cayman Islands: Conservation issues in the face of invasions, pp. 129–147. *In* A. Hailey, B. S. Wilson, and J. A. Horrocks (eds.), Conservation of Caribbean Island Herpetofaunas, Vol. 2. Regional Accounts of the West Indies. Brill, Leiden, Netherlands.

Farallo, V. R. and Forstner, M. R. J. 2012. Predation and the Maintenance of Color Polymorphism in a Habitat Specialist Squamate. *PLOS ONE* 7:e30316.

Garman, S. 1887. On the Reptiles and Batrachians of Grand Cayman. *Proceedings of the American Philosophical Society* 24:273–277.

Gelman, A. 2006. Prior distributions for variance parameters in hierarchical models (comment on article by Browne and Draper). *Bayesian Analysis* 1:515–534.

Gelman, A., Carlin, J. B., Stern, H. S., Dunson, D. B., Vehtari, A., and Rubin, D. B. 2013. Bayesian Data Analysis, Third Edition. CRC Press, Boca Raton, FL.

Gelman, A., Lee, D., and Guo, J. 2015. Stan A Probabilistic Programming Language for Bayesian Inference and Optimization. *Journal of Educational and Behavioral Statistics* 40:530–543.

Grant, C. and Lewis, C. B. 1940. The herpetology of the Cayman Islands. *Bulletin of the Institute of Jamaica, Science Series* 2:1–5.

Gray, S. M. and McKinnon, J. S. 2007. Linking color polymorphism maintenance and speciation. *Trends in Ecology & Evolution* 22:71–79.

Hijmans, R. J., Cameron, S. E., Parra, J. L., Jones, P. G., and Jarvis, A. 2005. Very high resolution interpolated climate surfaces for global land areas. *International Journal of Climatology* 25:1965–1978.

Hoffman, M. D. and Gelman, A. 2011. The No-U-Turn Sampler: Adaptively Setting Path Lengths in Hamiltonian Monte Carlo. *arXiv:1111.4246 [cs, stat]* . arXiv: 1111.4246.

Jackman, T. R., Irschick, D. J., De Queiroz, K., Losos, J. B., and Larson, A. 2002. Molecular phylogenetic perspective on evolution of lizards of the *Anolis grahami* series. *Journal of Experimental Zoology* 294:1–16.

Jones, B. 1994. Geology of the Cayman Islands, pp. 13–49. *In* M. A. Brunt and J. E. Davies (eds.), The Cayman Islands, number 71 in Monographiae Biologicae. Springer Netherlands. DOI: 10.1007/978-94-011-0904-8_2.

Kolbe, J. J., Larson, A., and Losos, J. B. 2007. Differential admixture shapes morphological variation among invasive populations of the lizard *Anolis sagrei*. *Molecular Ecology* 16:1579–1591.

Kolbe, J. J. and Losos, J. B. 2005. Hind-Limb Length Plasticity in *Anolis carolinensis*. *Journal of Herpetology* 39:674–678.

Kusche, H., Elmer, K. R., and Meyer, A. 2015. Sympatric ecological divergence associated with a color polymorphism. *BMC Biology* 13:82.

Lewandowski, D., Kurowicka, D., and Joe, H. 2009. Generating random correlation matrices based on vines and extended onion method. *Journal of Multivariate Analysis* 100:1989–2001.

Losos, J. 2011. Lizards in an Evolutionary Tree: Ecology and Adaptive Radiation of Anoles. University of California Press, Berkeley.

Losos, J. B. 1994. Integrative Approaches to Evolutionary Ecology: *Anolis* Lizards as Model Systems. *Annual Review of Ecology and Systematics* 25:467–493.

Losos, J. B., Jackman, T. R., Larson, A., de Queiroz, K., and Rodri?guez-Schettino, L. 1998. Contingency and Determinism in Replicated Adaptive Radiations of Island Lizards. *Science* 279:2115–2118.

Losos, J. B., Marks, J. C., and Schoener, T. W. 1993. Habitat use and ecological interactions of an introduced and a native species of *Anolis* lizard on Grand Cayman, with a review of the outcomes of anole introductions. *Oecologia* 95:525–532.

Macedonia, J. M. 2001. Habitat light, colour variation, and ultraviolet reflectance in the Grand Cayman anole, *Anolis conspersus*. *Biological Journal of the Linnean Society* 73:299–320.

Macedonia, J. M. and Clark, D. L. 2001. Headbob Display Analysis of the Grand Cayman Anole, *Anolis conspersus*. *Journal of Herpetology* 35:300–310.

Malhotra, A. and Thorpe, R. S. 1997. Microgeographic Variation in Scalation of *Anolis oculatus* (Dominica, West Indies): A Multivariate Analysis. *Herpetologica* 53:49–62.

McElreath, R. 2016. Statistical Rethinking: A Bayesian Course with Examples in R and Stan. CRC Press, Boca Raton, FL.

Minton, S. A. and Minton, M. R. 1984. Geographic distribution. *Anolis sagrei. Herpetological Review* 15:77.

Muñoz, M. M., Crawford, N. G., McGreevy, T. J., Messana, N. J., Tarvin, R. D., Revell, L. J., Zandvliet, R. M., Hopwood, J. M., Mock, E., Schneider, A. L., and Schneider, C. J. 2013. Divergence in coloration and ecological

speciation in the Anolis marmoratus species complex. *Molecular Ecology* 22:2668–2682.

Papaspiliopoulos, O., Roberts, G. O., and Sköld, M. 2007. A General Framework for the Parametrization of Hierarchical Models. *Statistical Science* 22:59–73.

Plant, R. E. 2012. Spatial Data Analysis in Ecology and Agriculture Using R. CRC Press, Boca Raton, FL.

R Core Team 2016. R: A Language and Environment for Statistical Computing. R Foundation for Statistical Computing, Vienna, Austria.

Runemark, A., Hansson, B., Pafilis, P., Valakos, E. D., and Svensson, E. I. 2010. Island biology and morphological divergence of the Skyros wall lizard *Podarcis gaigeae*: a combined role for local selection and genetic drift on color morph frequency divergence? *BMC Evolutionary Biology* 10:269.

Ryan, P. G., Moloney, C. L., and Hudon, J. 1994. Color Variation and Hybridization among *Nesospiza* Buntings on Inaccessible Island, Tristan da Cunha. *The Auk* 111:314–327.

Schoener, T. W. 1967. The Ecological Significance of Sexual Dimorphism in Size in the Lizard *Anolis conspersus*. *Science* 155:474–477.

Sigmund, W. R. 1983. Female Preference for *Anolis carolinensis* Males as a Function of Dewlap Color and Background Coloration. *Journal of Herpetology* 17:137–143.

Sinervo, B., Bleay, C., and Adamopoulou, C. 2001. Social Causes of Correlational Selection and the Resolution of a Heritable Throat Color Polymorphism in a Lizard. *Evolution* 55:2040–2052.

Thorpe, R. S. and Stenson, A. G. 2003. Phylogeny, paraphyly and ecological adaptation of the colour and pattern in the *Anolis roquet* complex on Martinique. *Molecular Ecology* 12:117–132.

Tibshirani, R. 1996. Regression Shrinkage and Selection via the Lasso. *Journal of the Royal Statistical Society. Series B (Methodological)* 58:267–288.

Truong, H. 2012. Coloration in relation to ecology in the Asian spiny-backed spider, *Thelacantha brevispina* (Araneae, Araneidae) on Moorea, French Polynesia. *eScholarship* Student Research Papers, Fall 2012.

Tuttle, E. M. 2003. Alternative reproductive strategies in the white-throated sparrow: behavioral and genetic evidence. *Behavioral Ecology* 14:425–432.

van Etten, J. 2015. gdistance: Distances and Routes on Geographical Grids. R package version 1.1-9. https://CRAN.R-project.org/package=gdistance.

Williams, E. E. 1972. The Origin of Faunas. Evolution of Lizard Congeners in a Complex Island Fauna: A Trial Analysis, pp. 47–89. *In* T. Dobzhansky, M. K. Hecht, and W. C. Steere (eds.), Evolutionary Biology. Springer US. DOI: 10.1007/978-1-4684-9063-3_3.

Zou, H. and Hastie, T. 2005. Regularization and variable selection via the elastic net. *Journal of the Royal Statistical Society: Series B (Statistical Methodology)* 67:301–320.

Appendices

A Tables

Table A.1: Study Locations

Site	Latitude	Longitude
A	19°22’35" N	81°25’00" W
B	19°16’51" N	81°23’32" W
C	19°17’26" N	81°22’48" W
D	19°21’23" N	81°22’46" W
E	19°18’57" N	81°22’43" W
F	19°23’23" N	81°22’14" W
G	19°17’33" N	81°21’52" W
H	19°16’38" N	81°20’26" W
I	19°16’39" N	81°17’11" W
J	19°21’21" N	81°16’29" W
K	19°16’44" N	81°15’06" W
L	19°17’12" N	81°14’21" W
M	19°20’20" N	81°11’38" W
N	19°18’53" N	81°11’29" W
O	19°19’05" N	81°10’04" W
P	19°20’57" N	81°07’56" W
Q	19°18’05" N	81°06’36" W
R	19°19’40" N	81°06’11" W
S	19°21’03" N	81°05’55" W

Table A.2: Data and Indices in Model

Symbol	Value(s)	Description
n	303	Number of observations.
m	19	Number of sites.
d	18	Number of predictors (not including the intercept).
i	$\{1, 2, ..., n\}$	An individual observation (i.e., one lizard and its traits).
j	$\{1, 2, ..., m\}$	A sample site; each lizard belongs to one and only site.
k	$\{0, 1, ..., d\}$	A predictor in the model; when $k = 0$, this is the intercept.
$\boldsymbol{X}$	Varies	n by $d + 1$ matrix of predictors, where the first column is a vector of 1.
$\boldsymbol{Y}$	$\{0, 1\}$	n-length vector of binary responses.
$\boldsymbol{Z}$	Varies	m-length vector of site-level precipitation values.

Table A.3: Parameters in Pattern Model

Symbol	Support	Description
p_i	$(0, 1)$	Probability that $Y_i = 1$.
η_i	$(-\infty, \infty)$	Linear predictor for observation i.
$\beta_{j,k}$	$(-\infty, \infty)$	Coefficient for predictor k in site j. When $k = 0$, this is the intercept.
$\boldsymbol{\beta}_j$	$(-\infty, \infty)$	Vector of all β coefficients for site j.
μ_k	$(-\infty, \infty)$	Grand coefficient for predictor k.
σ_k	$(0, \infty)$	Standard deviation for dispersion of $\beta_{j,k}$ around μ_k.
τ_σ	$(0, \infty)$	Global scale parameter for σ_k.
λ_k	$(0, \infty)$	Standard deviation of μ_k.
τ_λ	$(0, \infty)$	Global scale parameter for λ_k.
$\boldsymbol{\Sigma}$	$(-\infty, \infty)$	Covariance matrix for $\boldsymbol{\beta}_j$, for correlation among a site's coefficients.
$\boldsymbol{\Omega}$	$(-1, 1)$	Correlation structure of Σ; $\Sigma = \sigma_{\text{diag}}\Omega\sigma_{\text{diag}}$, where $\sigma_{\text{diag}} = \text{diag}(\boldsymbol{\sigma})$.
ϕ	$(0, \infty)$	Parameter for LKJ distribution.
$\boldsymbol{\beta}^*_j$	$(-\infty, \infty)$	β_j, modified to account for the effect of γZ_j on $\beta_{j,0}$.
γ	$(-\infty, \infty)$	Coefficient for effect of Z_j on $\beta^*_{j,0}$.
ξ	$(0, \infty)$	Standard deviation of γ.
$\boldsymbol{\Psi}$	$(0, 1)$	Spatial correlation matrix among sites.
$\boldsymbol{D_{j,j'}}$	$(0, \infty)$	Spatial distance between sites j and j'.
ℓ	$(0, \infty)$	Rate of spatial autocorrelation decay.

Table A.4: Parameters in Hierarchical Means Model

Symbol	Support	Description
α_j	$(-\infty, \infty)$	Mean of trait $\boldsymbol{X}_k$ at site j.
θ_j	$(-\infty, \infty)$	Expected value of α_j.
ω	$(-\infty, \infty)$	Grand mean of $\boldsymbol{X}_k$.
τ_α	$(0, \infty)$	Scale for dispersion of α_j around θ_j.
δ	$(-\infty, \infty)$	Coefficient for the effect of Z_j on α_j.
τ_δ	$(0, \infty)$	Scale parameter for δ.
ε_i	$(0, \infty)$	Scale of dispersion of $\boldsymbol{X}_k$ around α at site j.
τ_ε	$(0, \infty)$	Global scale parameter for ε_j.
q_x	Fixed	One-quarter of the sample range of $\boldsymbol{X}_k$.
c_x	Fixed	Sample median of $\boldsymbol{X}_k$.

B Figures

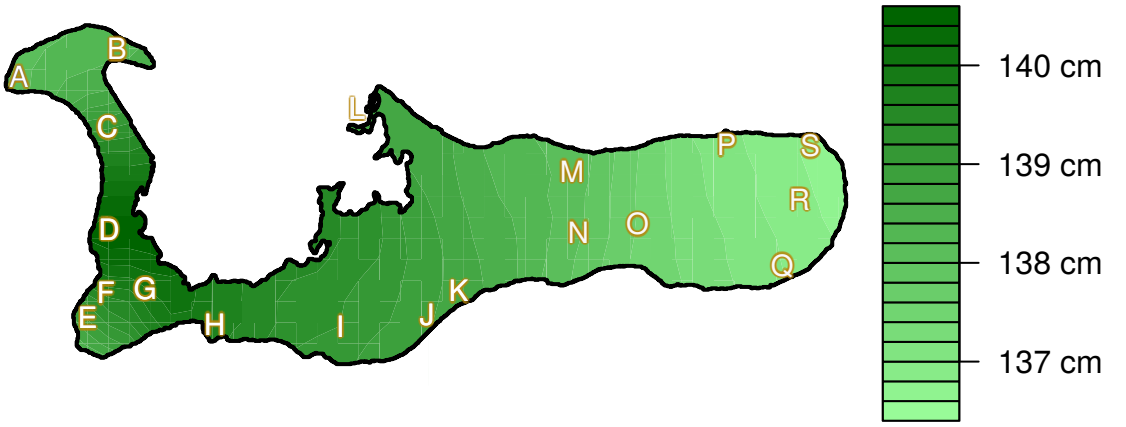

Figure B.1: Map of study sites on Grand Cayman, with average annual precipitation (WORLDCLIM climate layers; Hijmans et al., 2005)

Figure B.2: Logistic regression model.

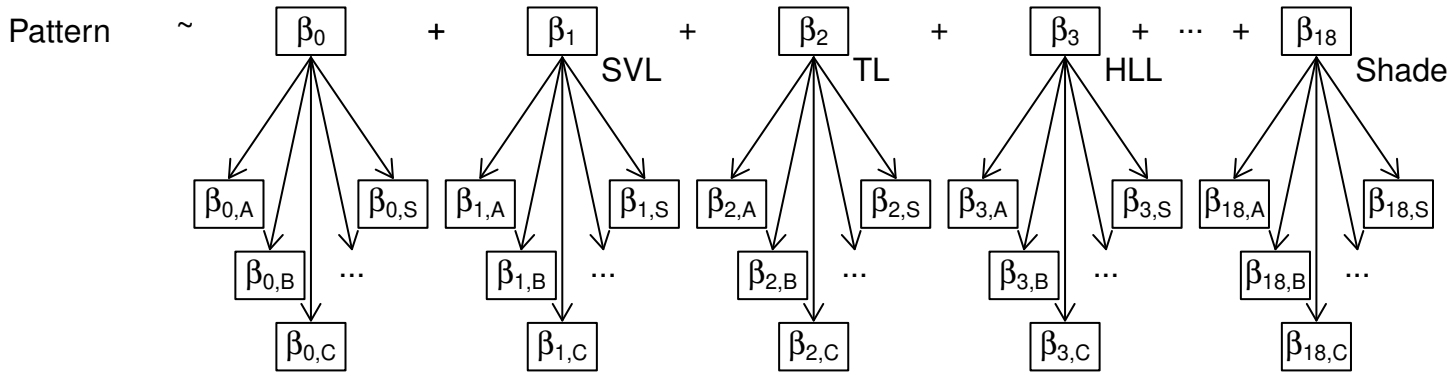

Figure B.3: Hierarchical logistic regression model with coefficient variation among sites.

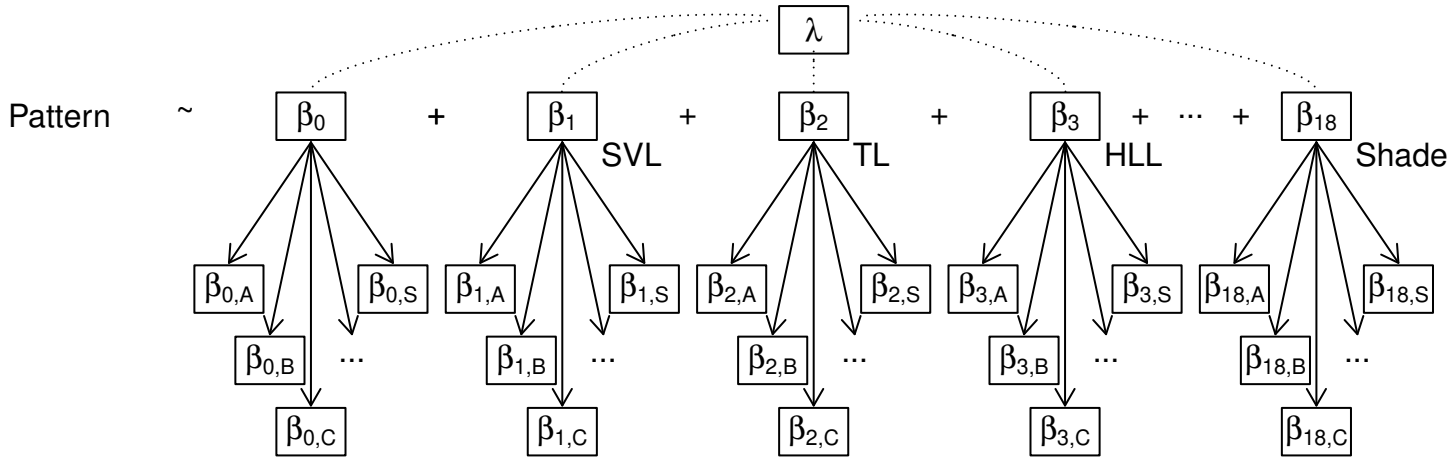

Figure B.4: Hierarchical logistic regression model with shrinkage priors for regularization and model selection.

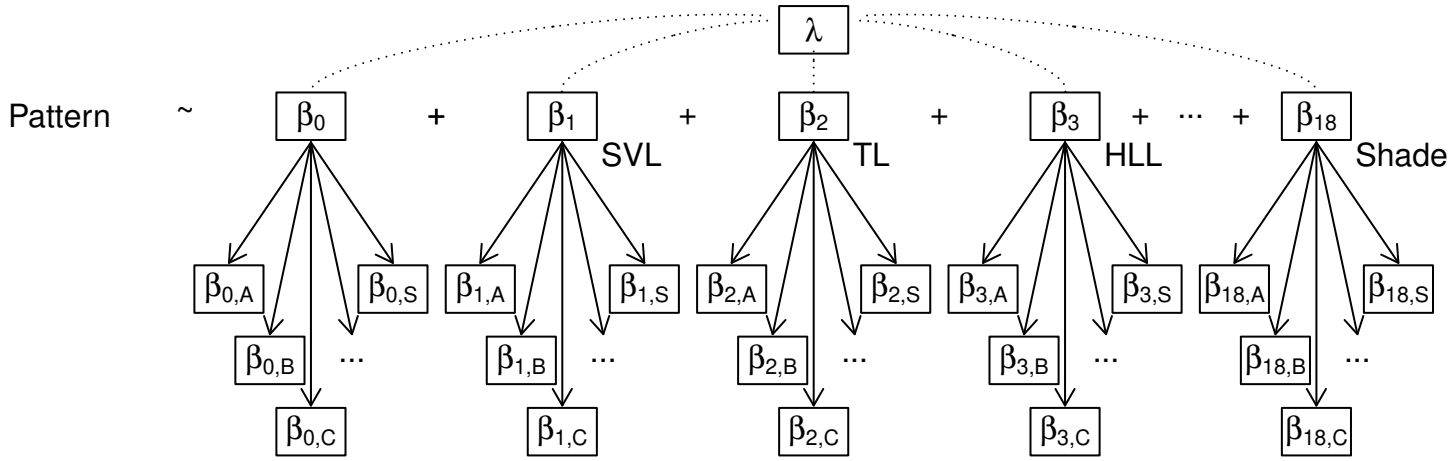

Figure B.5: Hierarchical logistic regression model with regularization and a site-level covariate (precipitation).

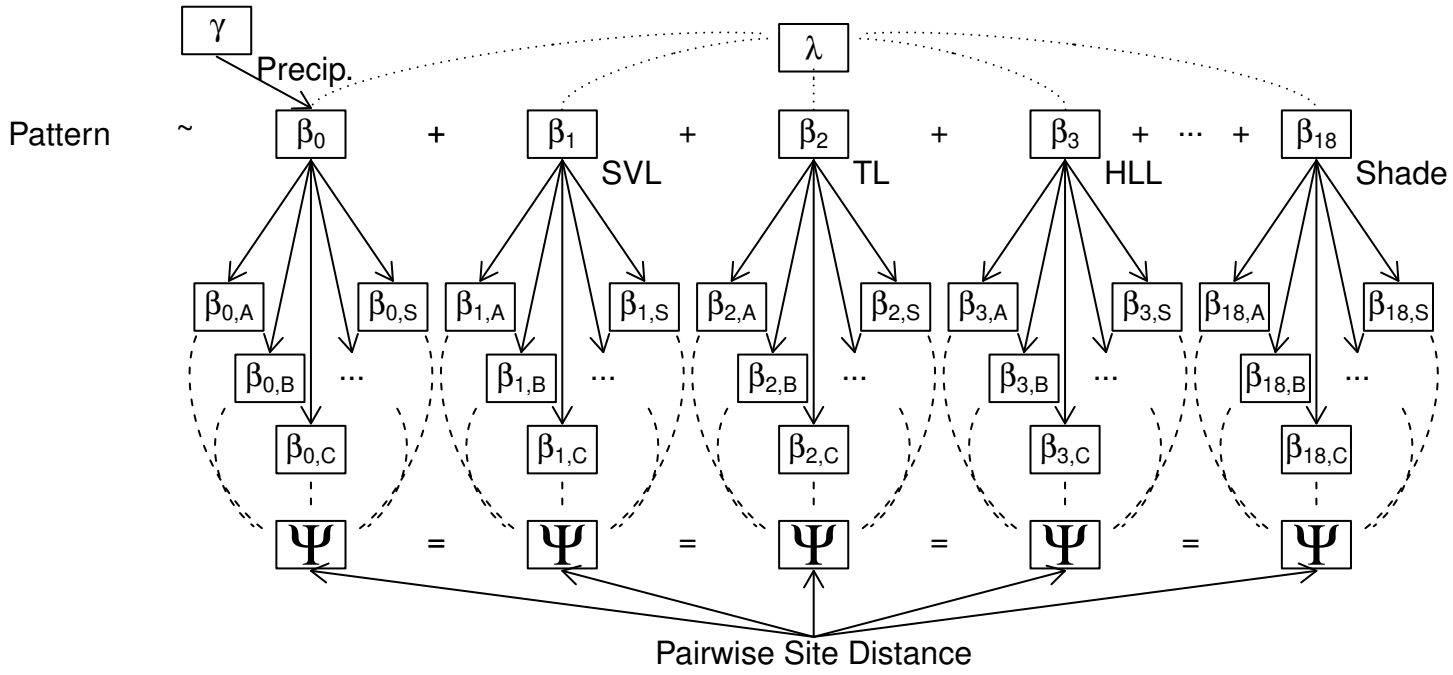

Figure B.6: Hierarchical logistic regression model with regularization, site-level effects, and spatial autocorrelation among sites.

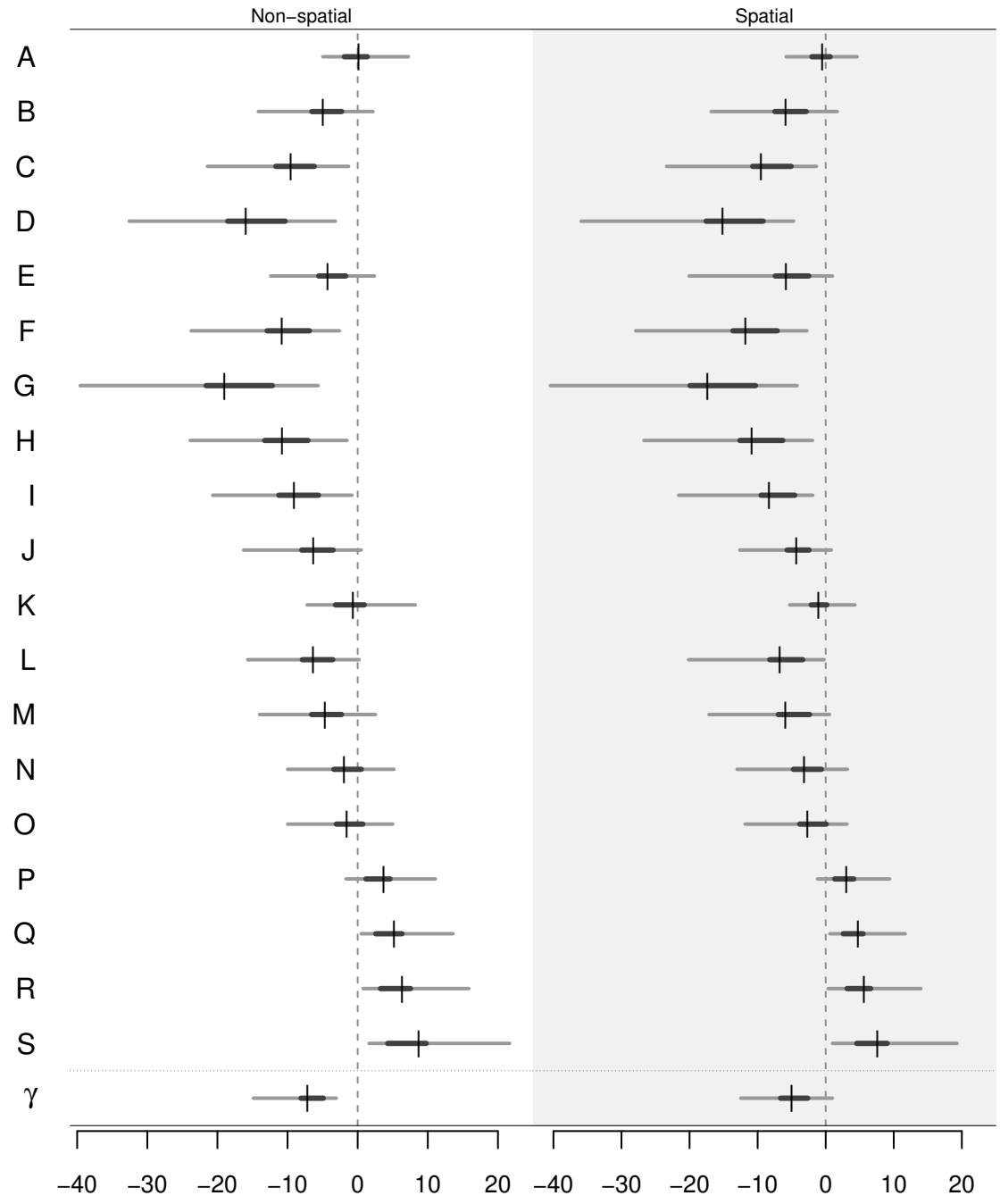

Figure B.7: Intercepts for the spatial (right) and non-spatial (left) pattern models at each site (A-S), indicating the log-odds of being spotted (negative) or vermiculated (positive). γ is the coefficient for the effect of precipitation on these intercepts. Each coefficient is represented by the 95% (light gray bar) and 50% (dark gray bar) high-density interval (HDI) and median (vertical bar) of the parameter's posterior distribution.

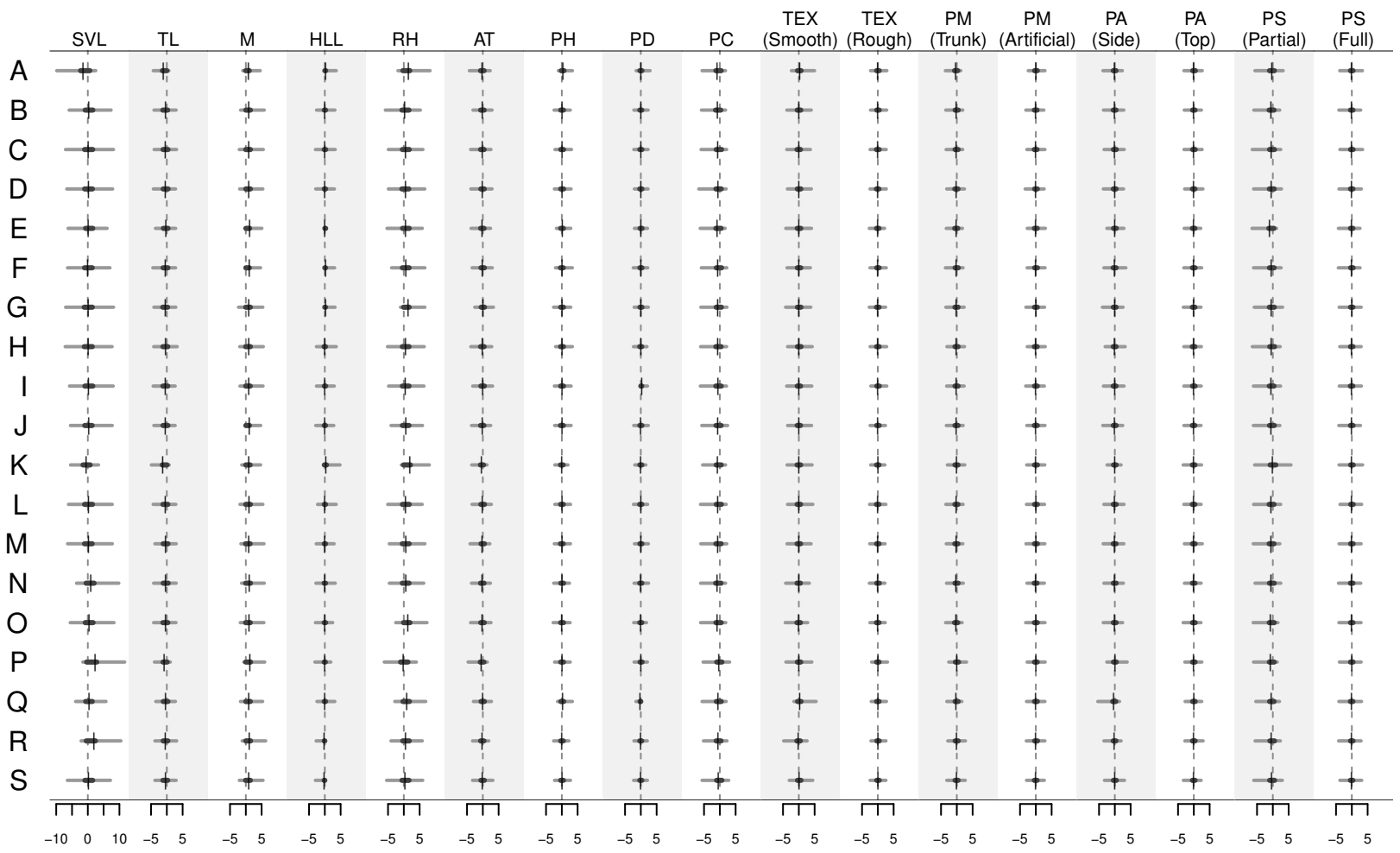

Figure B.8: Slopes of the non-spatial pattern model for each predictor (columns) at each site (rows), indicating the log-odds of being spotted (negative) or vermiculated (positive). Each coefficient is represented by the 95% (light gray bar) and 50% (dark gray bar) high-density interval (HDI) and median (vertical bar) of the parameter's posterior distribution.

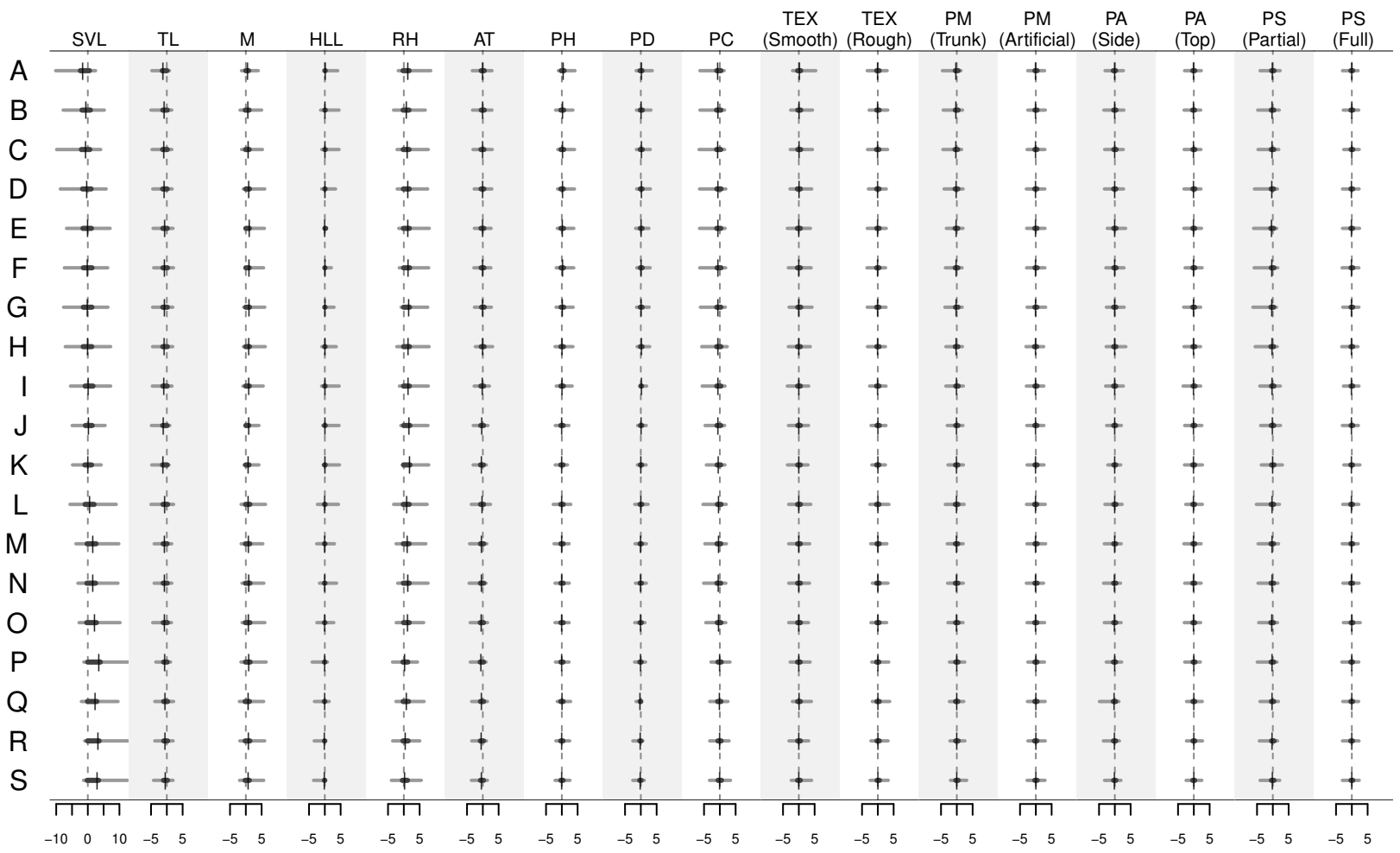

Figure B.9: Slopes of the spatial pattern model for each predictor (columns) at each site (rows), indicating the log-odds of being spotted (negative) or vermiculated (positive). Each coefficient is represented by the 95% (light gray bar) and 50% (dark gray bar) high-density interval (HDI) and median (vertical bar) of the parameter's posterior distribution.

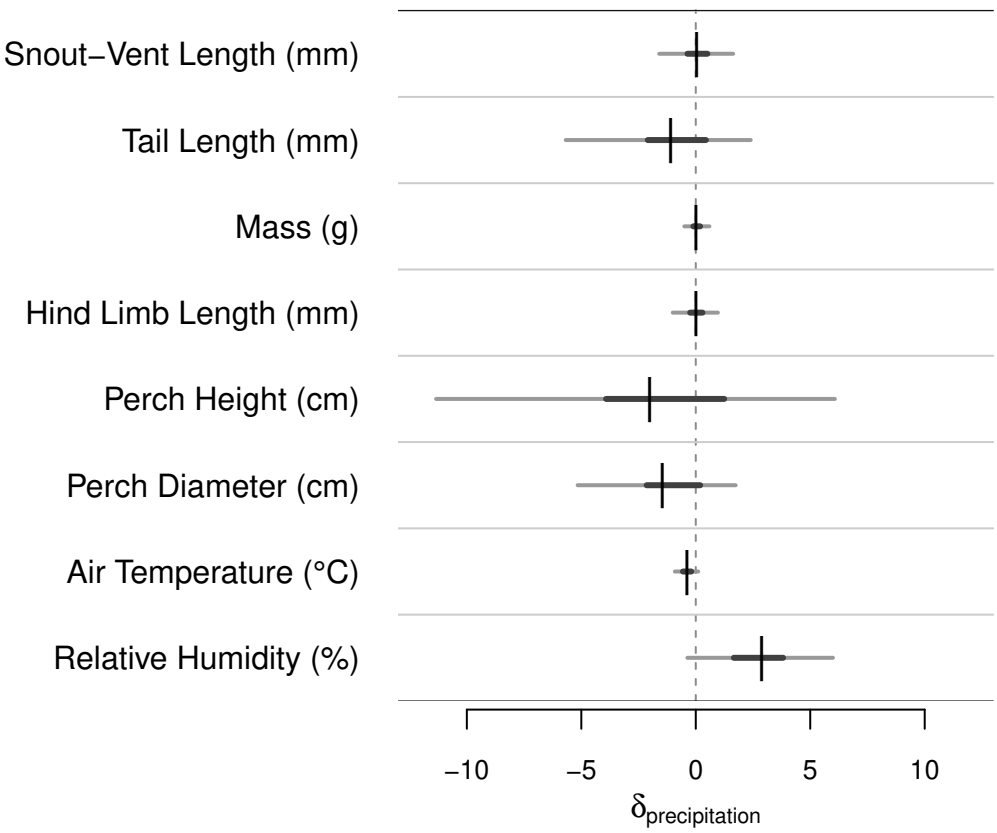

Figure B.10: The effect of precipitation on the site-level means of each continuous trait. Each coefficient is represented by the 95% (light gray bar) and 50% (dark gray bar) high-density interval (HDI) and median (vertical bar) of the parameter's posterior distribution.

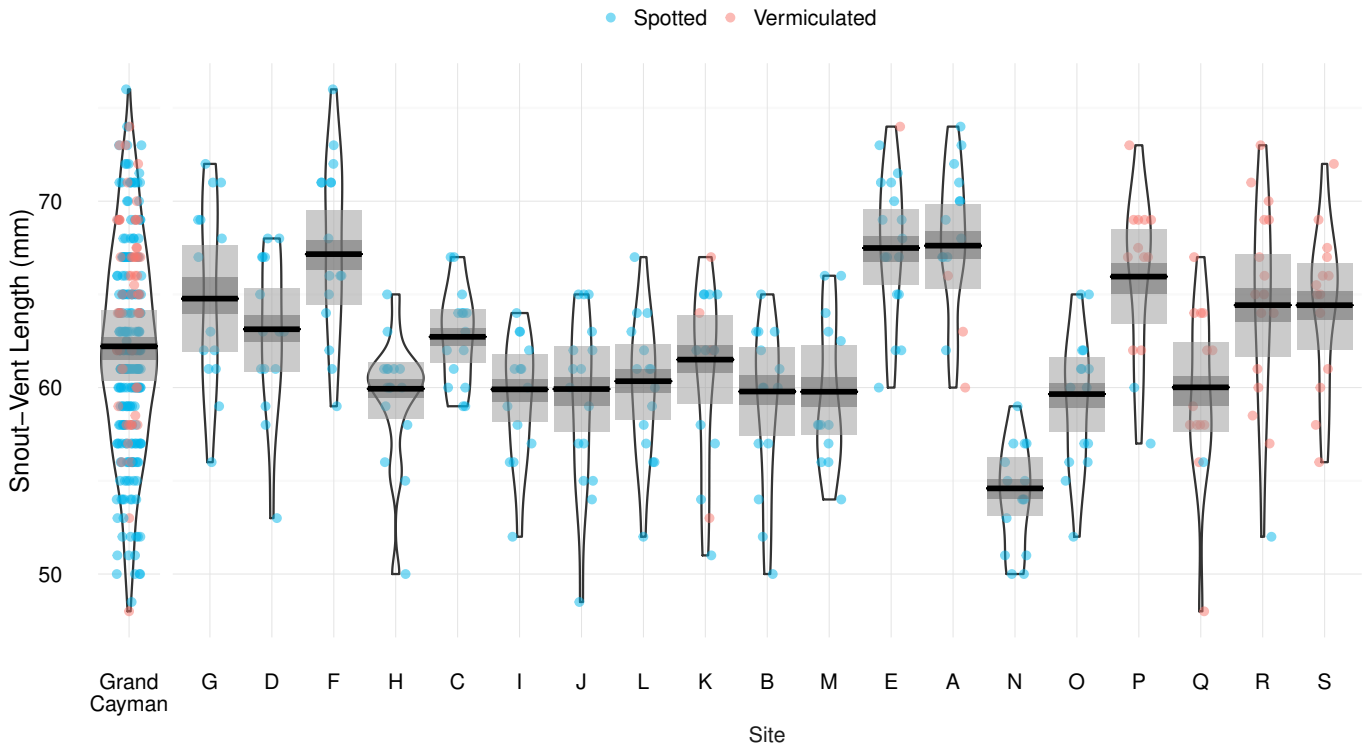

Figure B.11: Snout-vent length at each site, with nonparametric kernel density estimates and site means (light gray: 95% HDI; dark gray: 50% HDI; black: median). Sites are ordered from greatest (G) to least (S) annual precipitation.

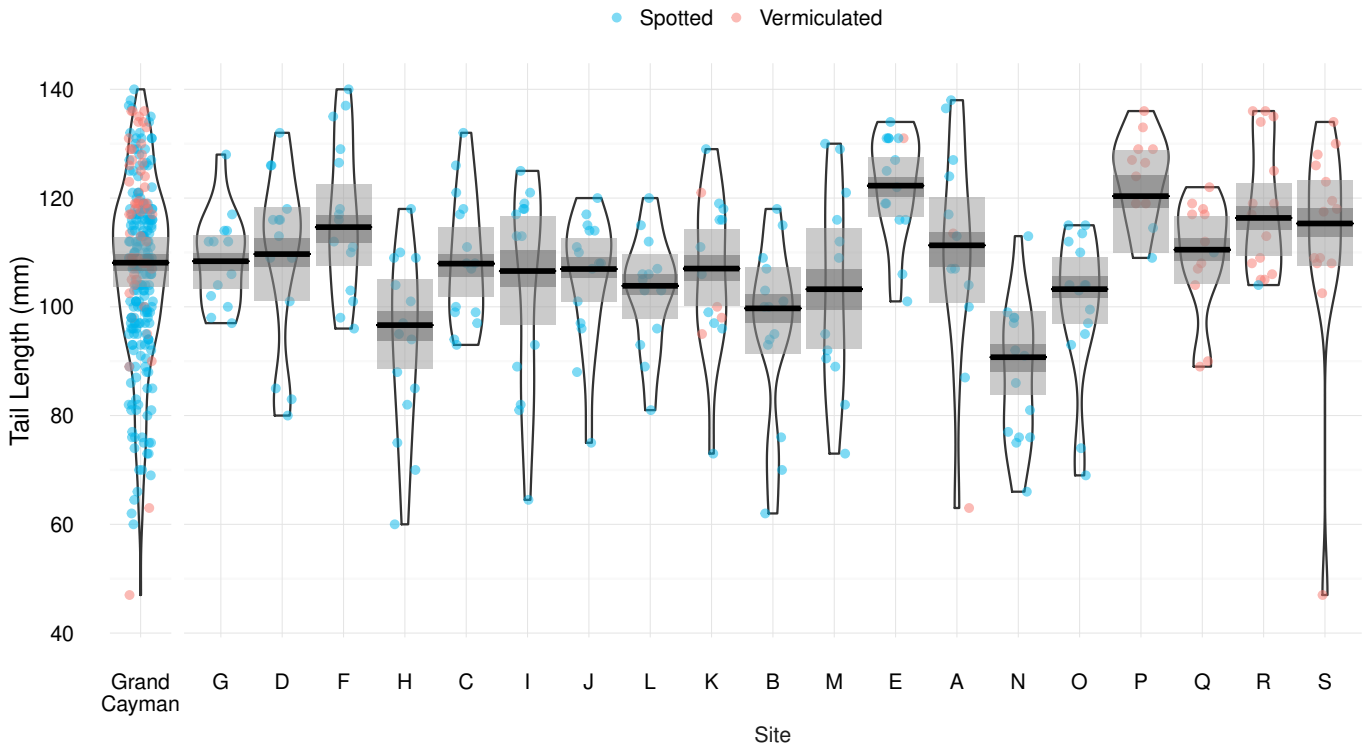

Figure B.12: Tail length at each site, with nonparametric kernel density estimates and site means (light gray: 95% HDI; dark gray: 50% HDI; black: median). Sites are ordered from greatest (G) to least (S) annual precipitation.

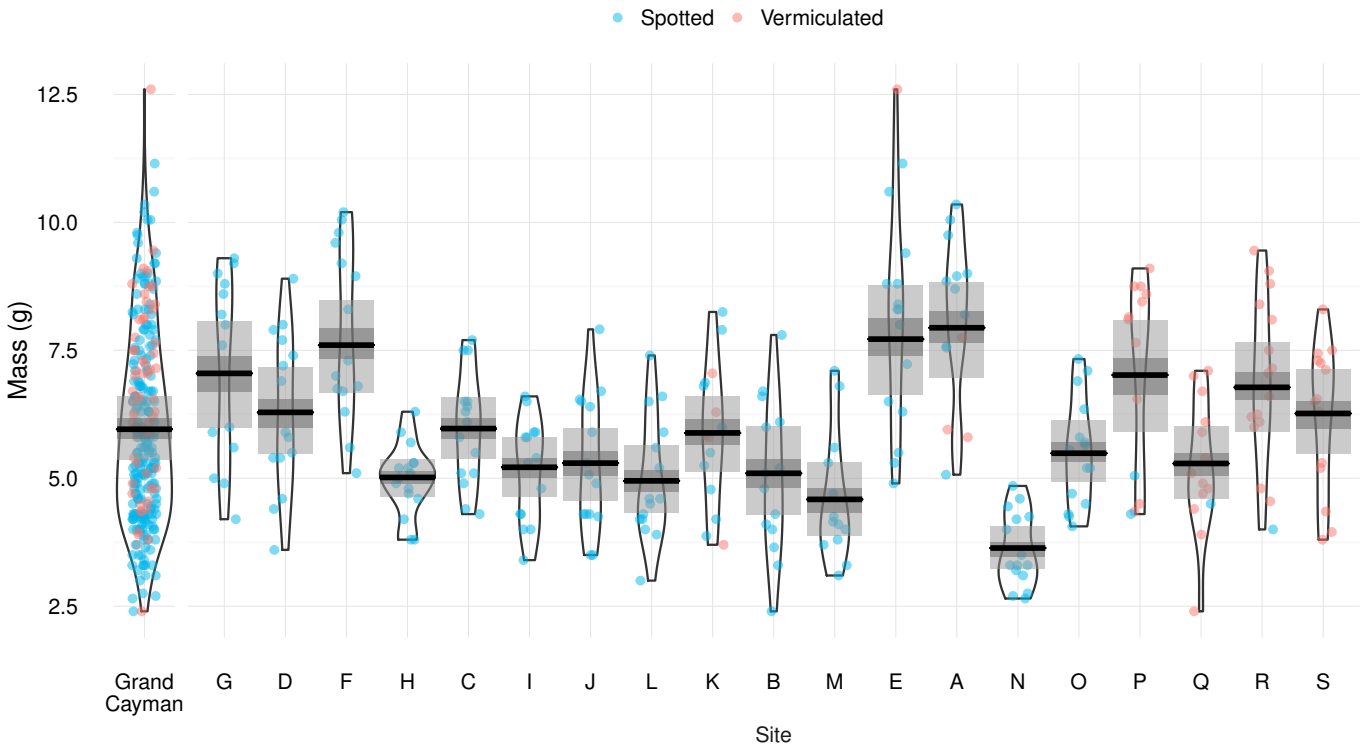

Figure B.13: Mass at each site, with nonparametric kernel density estimates and site means (light gray: 95% HDI; dark gray: 50% HDI; black: median). Sites are ordered from greatest (G) to least (S) annual precipitation.

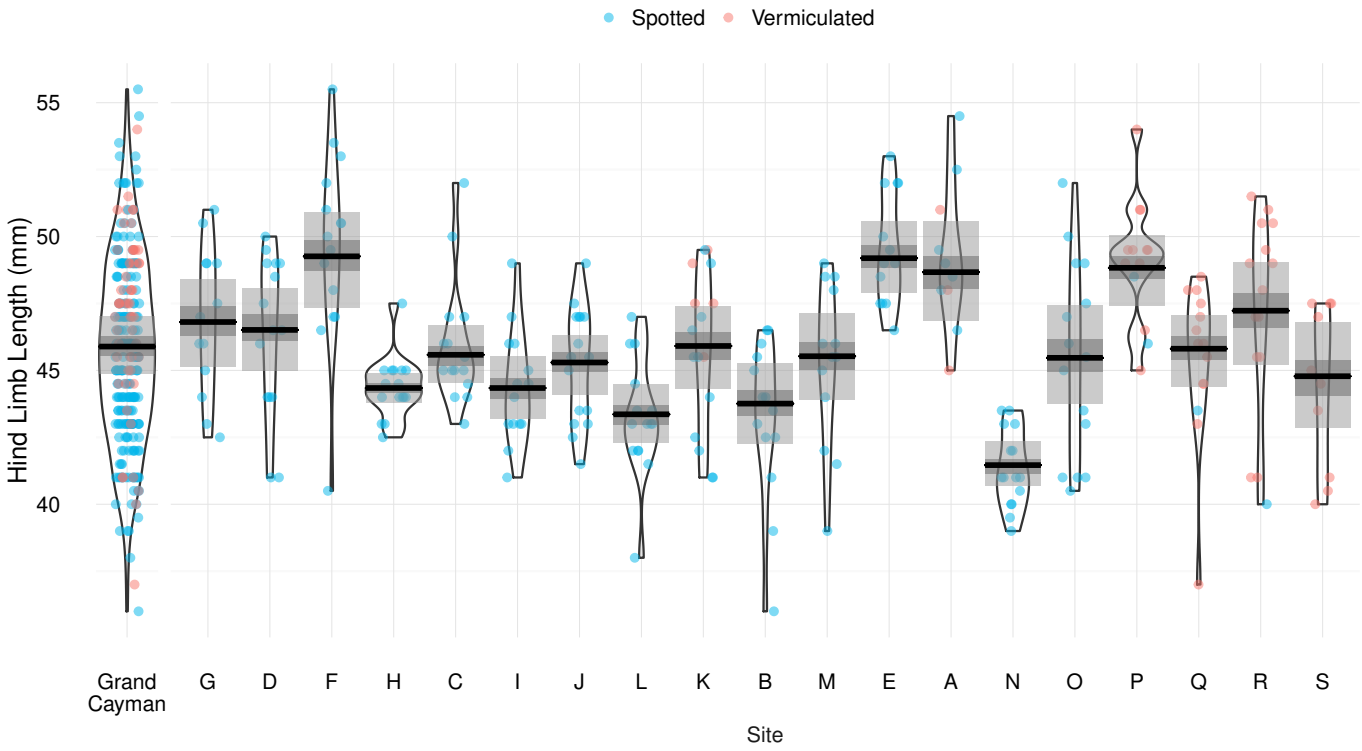

Figure B.14: Hind limb length at each site, with nonparametric kernel density estimates and site means (light gray: 95% HDI; dark gray: 50% HDI; black: median). Sites are ordered from greatest (G) to least (S) annual precipitation.

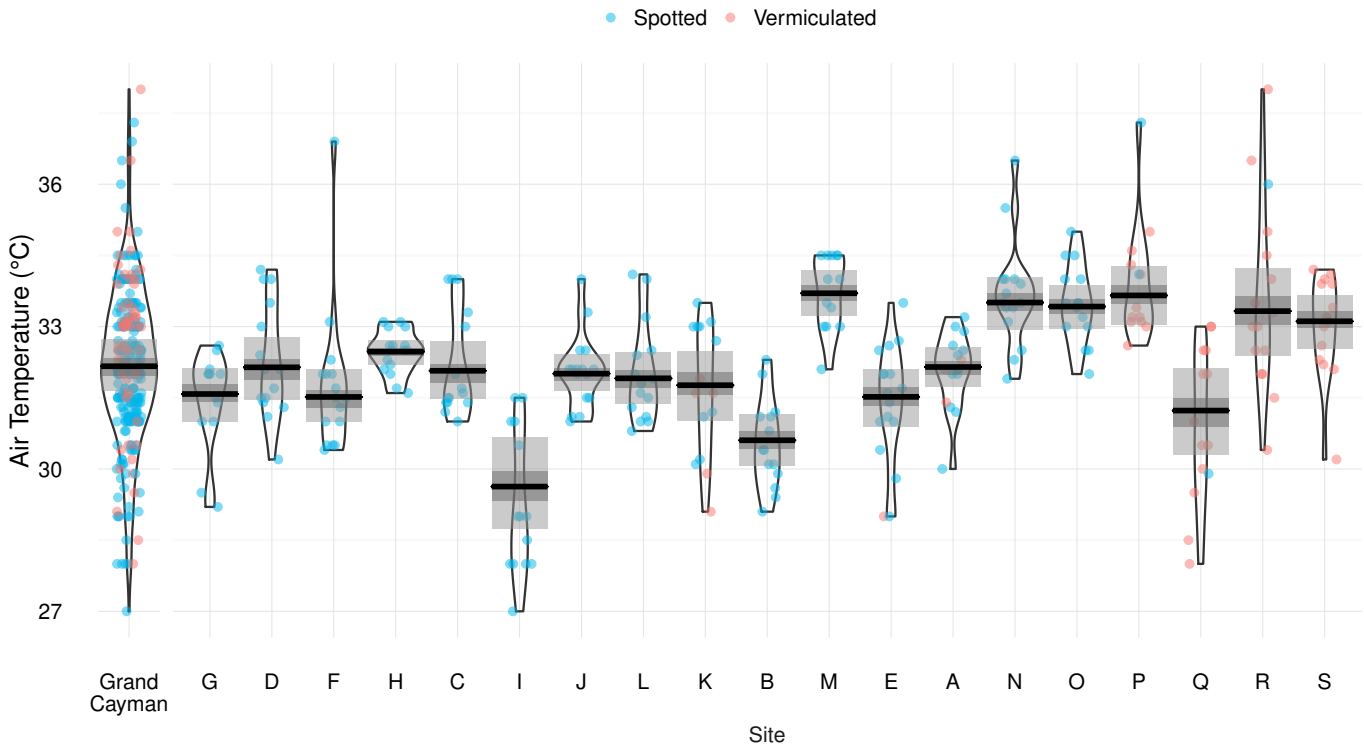

Figure B.15: Ambient air temperature at each site, with nonparametric kernel density estimates and site means (light gray: 95% HDI; dark gray: 50% HDI; black: median). Sites are ordered from greatest (G) to least (S) annual precipitation.

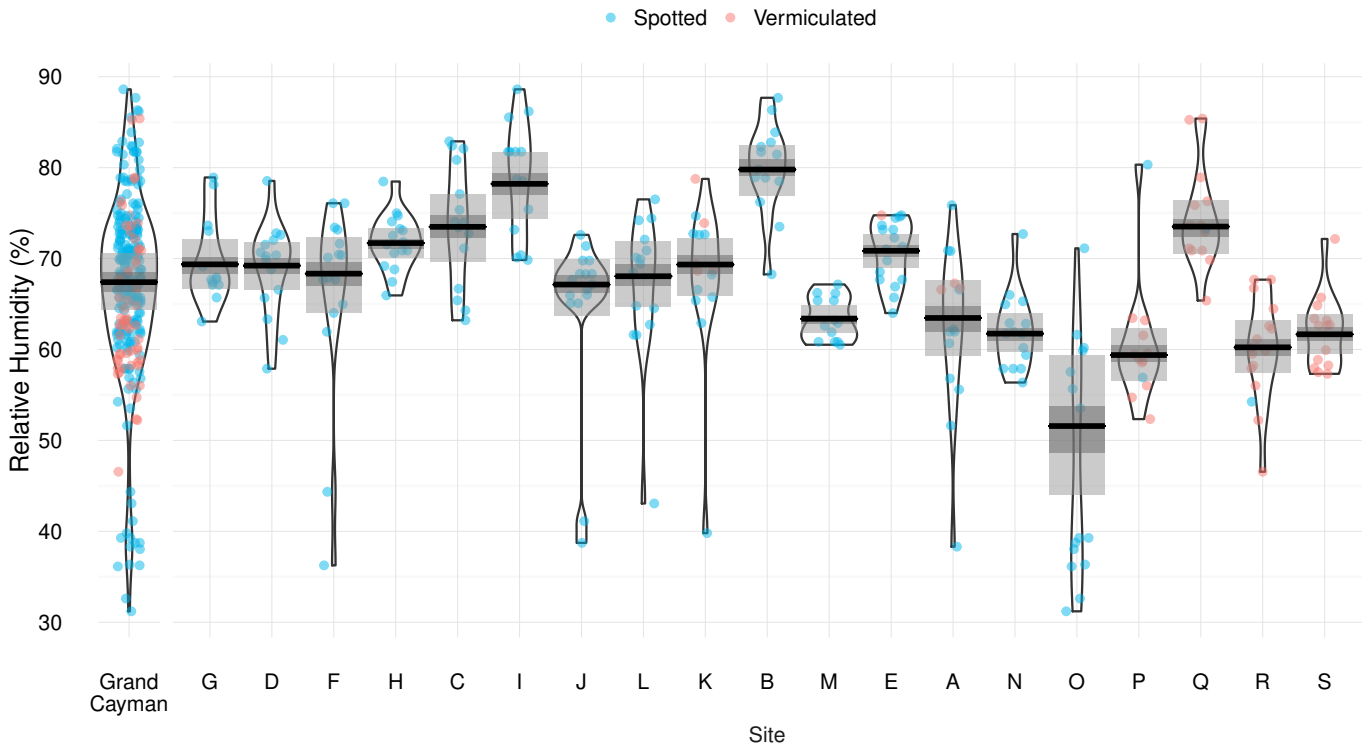

Figure B.16: Relative humidity at each site, with nonparametric kernel density estimates and site means (light gray: 95% HDI; dark gray: 50% HDI; black: median). Sites are ordered from greatest (G) to least (S) annual precipitation.

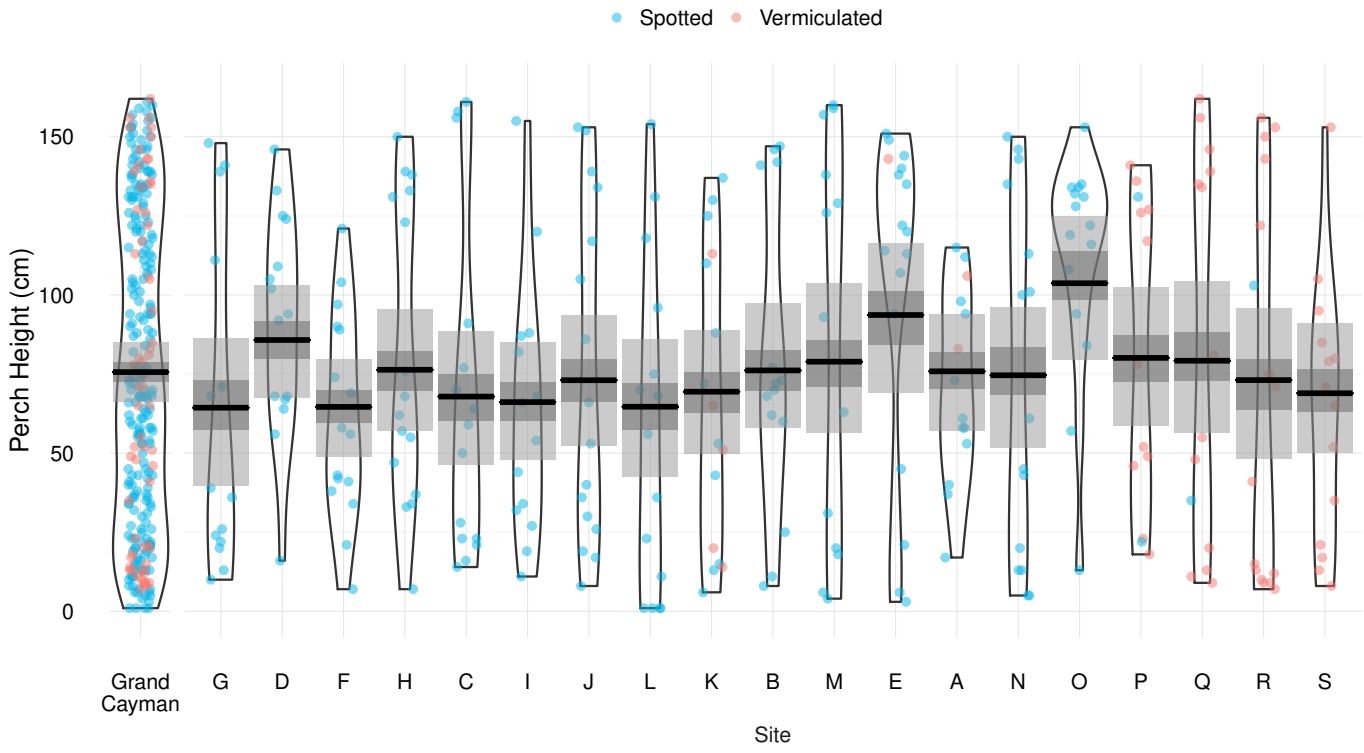

Figure B.17: Perch height at each site, with nonparametric kernel density estimates and site means (light gray: 95% HDI; dark gray: 50% HDI; black: median). Sites are ordered from greatest (G) to least (S) annual precipitation.

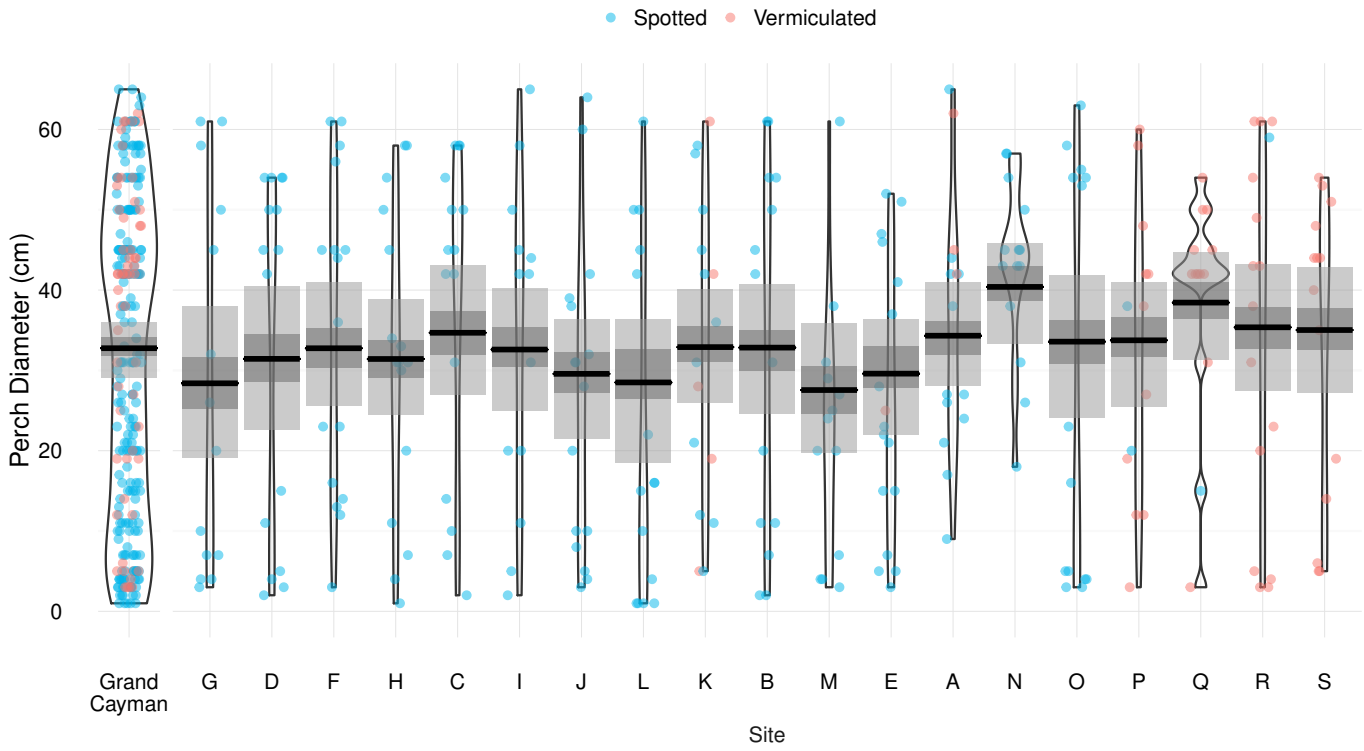

Figure B.18: Perch diameter at each site, with nonparametric kernel density estimates and site means (light gray: 95% HDI; dark gray: 50% HDI; black: median). Sites are ordered from greatest (G) to least (S) annual precipitation.

C Model Specifications

Non-Spatial Pattern Model

$$
\begin{aligned}
Y_i &\sim \text{Bernoulli}(p_i) \\
p_i &= \text{logit}^{-1}(\eta_i) \\
\eta_i &= \boldsymbol{\beta^*_{j|i}} \boldsymbol{X_i} \\
\beta^*_{j,k} &= \begin{cases} \beta_{j,k} + \gamma Z_j & k = 0 \\ \beta_{j,k} & k > 0 \end{cases} \\
\boldsymbol{\beta_j} &\sim \text{MVN}(\boldsymbol{\mu}, \Sigma) \\
\Sigma &= \text{diag}(\boldsymbol{\sigma}) \boldsymbol{\Omega} \text{diag}(\boldsymbol{\sigma}) \\
\boldsymbol{\Omega} &\sim \text{LKJ}(2) \\
\sigma_k &\sim \text{Cauchy}^+(0, \tau_\sigma) \\
\tau_\sigma &\sim \text{Cauchy}^+(0, 1) \\
\mu_k &\sim \text{Normal}(0, \lambda_k) \\
\lambda_k &= \lambda_{k,1} \lambda_{k,2} \\
\lambda_{k,\{1,2\}} &\sim t_3^+(0, \sqrt{\tau_\lambda}) \\
\tau_\lambda &\sim \text{Cauchy}^+(0, d^{-1}) \\
\gamma &\sim \text{Normal}(0, \xi) \\
\xi &\sim \text{Cauchy}^+(0, 2.5)
\end{aligned}
$$

Spatial Pattern Model

$$
\begin{aligned}
Y_i &\sim \text{Bernoulli}(p_i) \\
p_i &= \text{logit}^{-1}(\eta_i) \\
\eta_i &= \boldsymbol{\beta^*_{j|i}} \boldsymbol{X_i} \\
\beta^*_{j,k} &= \begin{cases} \beta_{j,k} + \gamma Z_j & k = 0 \\ \beta_{j,k} & k > 0 \end{cases} \\
\boldsymbol{\beta} &\sim \mathcal{MN}(\boldsymbol{\mu}, \boldsymbol{\Psi}, \Sigma) \\
\Sigma &= \text{diag}(\boldsymbol{\sigma}) \boldsymbol{\Omega} \text{diag}(\boldsymbol{\sigma}) \\
\boldsymbol{\Omega} &\sim \text{LKJ}(2) \\
\sigma_k &\sim \text{Cauchy}^+(0, \tau_\sigma) \\
\tau_\sigma &\sim \text{Cauchy}^+(0, 1) \\
\Psi_{j,j'} &= \exp\left(-\frac{D^2_{j,j'}}{\ell^2}\right) \\
\ell &\sim \text{Cauchy}^+(0, 1) \\
\mu_k &\sim \text{Normal}(0, \lambda_k) \\
\lambda_k &= \lambda_{k,1} \lambda_{k,2} \\
\lambda_{k,\{1,2\}} &\sim t_3^+(0, \sqrt{\tau_\lambda}) \\
\tau_\lambda &\sim \text{Cauchy}^+(0, d^{-1}) \\
\gamma &\sim \text{Normal}(0, \xi) \\
\xi &\sim \text{Cauchy}^+(0, 2.5)
\end{aligned}
$$

$=$ indicates a deterministic relationship

$\sim$ indicates a stochastic relationship

Hierarchical Trait Means Model

$$
\begin{aligned}
X_i &\sim t_7(\alpha_{j|i}, \varepsilon_{j|i}) \\
\alpha_j &\sim \text{Normal}(\theta_j, \tau_\alpha) \\
\theta_j &= \omega + \delta Z_j \\
\omega &\sim \text{Normal}(c_x, q_x) \\
\tau_\alpha &\sim \text{Cauchy}^+(0, q_x) \\
\delta &\sim \text{Normal}(0, \tau_\delta) \\
\tau_\delta &\sim \text{Cauchy}^+(0, q_x) \\
\varepsilon_j &\sim \text{Cauchy}^+(0, \tau_\varepsilon) \\
\tau_\varepsilon &\sim \text{Cauchy}^+(0, q_x) \\
q_x &= \text{Range}(X)/4 \\
c_x &= \text{Median}(X)
\end{aligned}
$$

$=$ indicates a deterministic relationship

$\sim$ indicates a stochastic relationship

Vita

Christopher R. Peterson was born in Starkville, MS in 1991 and moved to Ocean Springs, MS at the age of three. As the son of two marine biologists, Christopher frequently attended the annual meetings of the American Society of Ichthyologists and Herpetologists, spurring his decision to become an ecologist. After graduating from Ocean Springs High School in 2009, he attended the University of Arkansas for a B.S. in Biological Sciences. As an undergraduate, Christopher studied the effects of gastrointestinal microbes on snake digestion under the guidance Steven Beaupre. From 2013 to 2016, he studied Ecology and Evolutionary Biology at the University of Tennessee under the guidance of Sandy Echternacht. Upon completion of his M.S. degree, Christopher will be attending University of Texas, Austin to work on a Ph.D. in Ecology, Evolution, and Behavior with Daniel Bolnick.